LIGHT PROPAGATION IN TISSUES WITH CONTROLLED OPTICAL PROPERTIES

Valery V. Tuchin,[†,‡] **Irina L. Maksimova,**[†,*] **Dmitry A. Zimnyakov,**[†,‡] **Irina L. Kon,**[**] **Albert H. Mavlutov,**[†] **and Alexey A. Mishin**[‡]

[†]Saratov State University, Astrakhanskaya 83, Saratov 410026, Russia; [‡]Russian Academy of Science, Institute of Precision Mechanics and Control, Rabochaya 24, Saratov 410028, Russia; [*]Russian Academy of Science, Institute of Radio Engineering and Electronics, Saratov Branch, Saratov 410019, Russia; [**]Saratov Medical University, Saratov 410071, Russia

ABSTRACT

Theoretical and computer modeling approaches, such as Mie theory, radiative transfer theory, diffusion wave correlation spectroscopy, and Monte Carlo simulation were used to analyze tissue optics during a process of optical clearing due to refractive index matching. Continuous wave transmittance and forward scattering measurements as well as intensity correlation experiments were used to monitor tissue structural and optical properties. As a control, tissue samples of the human sclera were taken. Osmotically active solutions, such as Trazograph, glucose, and polyethylene glycol, were used as chemicals. A characteristic time response of human scleral optical clearing the range 3 to 10 min was determined. The diffusion coefficients describing the permeability of the scleral samples to Trazograph were experimentally estimated; the average value was $D_T \approx (0.9 \pm 0.5) \times 10^{-5}$ cm^2/s. The results are general and can be used to describe many other fibrous tissues. © 1997 Society of Photo-Optical Instrumentation Engineers. [S1083-3668(97)00804-6]

Keywords light scattering; sclera; osmolytes; refractive index matching.

1 INTRODUCTION

As a scattering medium, tissue shows optical effects that are characteristic of turbid physical systems (see, for example, Ref. 1). It is well known that the turbidity of a dispersive physical system can be effectively controlled using an immersion effect (matching the refractive indices of scatterers and the base material) as well as by changes in the size of scatterers and their packing (the volumetric arrangement affects the spatial correlation of the scatterers).[1–3] The optical (scattering) properties of living tissue can be controlled by using various physical and chemical reactions such as compression, stretching, dehydration, coagulation, UV irradiation, low-temperature application (reversible cold cataract), and addition of chemicals.[1,4–13]

Control of the optical properties of *in vivo* tissue is important for many applications. A number of laser surgery, therapy, and diagnostic technologies use tissue compression and stretching for better transport of the laser beam to underlying layers of tissue.[15] Compression of the human eye allows us to perform transscleral laser coagulation of the ciliary body and retina/choroid.[6] Selective clearing of the upper tissue layers would be very useful for developing eyeball diaphanoscopy techniques and for detecting local inhomogeneities hidden by a highly scattering medium in functional tomography.

Recently a number of results on noninvasive monitoring of glucose concentration within the human body using near infrared (NIR) light scattering techniques were reported.[12,13] The response of a nondiabetic male subject to a glucose load was measured by continuously monitoring the product $n\mu_s'$ (refractive index and reduced scattering coefficient) measured on muscle tissue of the subject's thigh.[11] In the human body, fluid homeostasis is maintained by a well-controlled balance of hydrostatic and osmotic pressures. This balance can be disturbed by certain physiological disorders induced by inflammation or trauma (lymphedema, burns, etc.) that leads to an easily detected change in tissue scattering properties in far red and NIR ranges.[14] The technologies developed (see Refs. 12–14) are very promising for noninvasive monitoring of bioliquids in living tissue. However, because of the random, inhomogeneous nature of the skin and underlying tissues (fat and muscle), which contain a number of chromophores, such technologies need detailed description and calibration for quantitative monitoring of glucose or other osmolytes.

On the other hand, tissues and fluids of the human eye, such as cornea, eye lens, sclera, and aqueous humor, may be considered as living optical eta-

---

Address all correspondence to Valery Tuchin. Tel: 8452 246036; Fax: 8452 240446; E-mail: tuchin@scnit.saratov.su

lons: the eye lens is a highly transparent medium in which scattering properties can vary dramatically under the influence of temperature, drugs, UV irradiation, etc.;[1,4,9,15] the cornea is a highly transparent medium with polarization anisotropy in which transmittance and polarization sensitivity can be effectively varied by the administration of immersion liquids[4,5]; the aqueous humor is a very promising biological fluid that shows quite good sensitivity to physiological concentrations of glucose in the human body.[16] Finally, the human sclera seems to be a good living scattering etalon in the visible range, like a white glass. The attractiveness of these eye tissues for endogenous and exogenous monitoring of chemicals is indicated by the well-developed models and theories describing their structure and optical properties (see Refs. 1, 4, 5, 9, 15, 17–32). The question is: What is the time response of the eye tissues and fluids to metabolic or administered chemicals?

In this paper, we present theoretical and experimental results on the optical properties of the human sclera controlled by administering osmotically active chemicals, such as Trazograph, glucose, and polyethylene glycol. Administration of chemical agents induces diffusion of matter and as a result equalization of the refractive indices of collagen and ground material. So, in order to build a complete model of the phenomenon under consideration, we need to develop two approaches for solving optical and matter diffusion problems which should be in agreement with each other. Therefore, for a quantitative description of tissue optical properties and the matching effect of refractive indices, we used Mie theory and the Hart and Farrell approach,[18,19] which holds that pair correlation between neighboring scatterers arises as a result of a quasi-random spatial distribution of collagen fibrils (scatterers) assembled in a compact fibrous tissue. Radiative transfer theory and Monte Carlo simulation were used to account for multiple scattering effects, which are especially important for untreated sclera and for the first stages of tissue optical clearing. For a description of coherent light scattering effects that allows us to understand the structural changes in controlled tissue, we used the appropriate spatial speckle correlometry technique based on random walk theory for complex amplitude fluctuations of the scattered field. The matter diffusion equation and irreversible thermodynamic approach were used to analyze the dynamics of chemical diffusion and osmotic phenomena in tissue. The use of the approaches developed to estimate the diffusion coefficients of chemical agents was demonstrated.

All experiments were performed *in vitro* using samples of the human sclera obtained from autopsy eyes. Optical transmission and reflection spectra as well as the dynamic response of scleral transmittance at the selected wavelengths were measured after osmotically active chemical agents were administered. The autocorrelation and structural functions of the far-zone speckle intensity fluctuations caused by scanning the sample perpendicular to the focused laser beam were recorded for different stages of tissue optical clearing (different time periods for administration of chemical agents). The evolution of the scattering coefficient variation and multiple-single scattering transition due to decay of scleral turbidity were demonstrated using the speckle technique. For direct confirmation of the osmotic nature of matching refractive indices, the sample's weight, the refractive indices of the chemical agents and the surrounding medium, as well as the osmotic pressure in the tissue were measured.

2 PHYSICAL PROPERTIES OF THE HUMAN SCLERA

The human sclera is a turbid, nontransparent medium that covers about 80% of the eyeball and serves as a protective membrane. Together with the cornea, it allows the eye to withstand both internal and external forces to maintain its shape. It is a strong, fibrous tissue that mainly consists of conjunctive collagen fibers packed in lamellar bundles[27,28,33] that are immersed in an amorphous ground (interstitial) substance containing glycosaminoglycans, proteins, and protein–polysaccharide complexes.[34,35] The glycosaminoglycans play a key role[34,35] in regulating the assembly of collagen fibrils and tissue permeability to water and other molecules.

The sclera contains three layers: the episclera, the stroma, and the lamina fusca.[6] The stroma is the thickest layer of the sclera. The thickness of the sclera and the arrangement of scleral collagen fibers show regional (limbal, equatorial, and posterior pole region) and aging differences.[28,33] In the equatorial region of the eye, collagen fibrils exhibit a wide range of diameters, from 25 to 230 nm.[33] The fibers in the scleral stroma have a diameter ranging from 30 to 300 nm.[6] Similar results for diameters have been obtained by other authors.[36,37] The fibrils' diameters[36,37] depend on age: they are the smallest in childhood.[36] The average diameter of the collagen fibrils increases gradually from about 65 nm in the innermost part to about 125 nm in the outermost part of the sclera;[28] the mean distance between fibril centers is about 285 nm.[38]

These fibrils are arranged in individual bundles in a parallel fashion but more randomly than that in the cornea; moreover, within each bundle, the groups of fibers are separated from each other by large empty lacunae randomly distributed in space.[33] Collagen bundles show a wide range of widths (1 to 50 μm) and thicknesses (0.5 to 6 μm) and tend to be wider and thicker toward the inner layers.[33] These ribbonlike structures are multiple cross-linked; their length can be a few millimeters.[6] They cross each other in all directions but remain

parallel to the scleral surface. The episclera has a similar structure with more randomly distributed and less compact bundles than in the stroma. The lamina fusca contains a larger amount of pigments, mainly melanin, which are generally located between the bundles. The sclera itself does not contain blood vessels but has a number of channels that allow arteries, veins, and nerves to enter or leave the eye.[6]

As was mentioned earlier, the thickness of the sclera is variable. It is thicker at the posterior pole (0.9 to 1.8 mm); it is thinnest at the equator (0.3–0.9 mm) and at the limbus is in the range of 0.5 to 0.8 mm.[6] The sclera reaches a maximum thickness at 30 to 40 years.[29] The age-averaged thickness for the posterior pole, the equator, and the limbus are 0.76, 0.45, and 0.56 mm (119 eyes, from 1 to 80 years old). For example, for the equator region, the thickness changes from 0.3 mm (1 year old) to 0.5 mm (30 to 40 years old), to 0.4 mm (70 years old). Hydration of the human sclera can be estimated as 68%. About 75% of its dry weight is due to collagen, 10% is due to other proteins, and 1% to mucopolysaccharides.[6]

In designing an optical model of the sclera, in addition to form, size, and density of the scatterers (fibrils) and the tissue thickness, it is important to have information on the refractive indices of the tissue components. For inhomogeneous materials, such as tissues, the refractive indices of fibrils, interstitial medium, and tissue can be derived using the law of Gladstone and Dale, which states that the resulting value represents an average of the refractive indices of the components related to their volume fractions.[6,18,27] where

$$n = \sum_{i=1}^{N} n_i V_i, \quad \sum_i V_i = 1, \tag{1}$$

n_i and V_i are the refractive index and volume fraction of the individual components, respectively, and N is the number of components.

Following Refs. 6, 27, 31, and 39, we can estimate the refractive index of the scleral fibrils (hydrated collagen) using the expression for the average refractive index of the sclera

$$n_s = n_C V_C + n_I V_I, \tag{2}$$

where n_C, n_I, and V_C, V_I are the refractive indices and volume fractions of the collagen and interstitial fluid between the fibers, respectively.

Because of the similar fibrous nature of the cornea and sclera (the differences are mainly due to distinctions in the fibril arrangements) it is expected that the refractive indices of scleral collagen and its interstitial fluid should be equal to those of the cornea. The refractive indices measured for dry corneal collagen and for the interstitial fluid are 1.547 and 1.342[6], respectively. Similar data for λ = 600 nm are presented in Refs. 27 and 39; for dry collagen it was measured as $n_c = 1.55$ and calculated

for the interstitial substance as $n_I = 1.345$. The results of direct measurement of the average refractive index of sclera using an Abbe refractometer are given in Ref. 6; $n_s = 1.385 \pm 0.005$ for λ = 589 nm. Using these data and (1) assuming that the refractive index for the scleral interstitial fluid $n_I = 1.345$, (2) that scleral hydration is about 68%, (3) that collagen makes up 75% of the dry weight, and (4) that the volume fraction of hydrated collagen is larger than for the dry collagen, $V_c = 0.31$ (instead of 0.24 for the dry collagen), on the basis of Eq. (2) we have obtained a refractive index of the scleral fibrils at λ = 600 nm, $n_c = 1.474$. These tendencies (changes of n_c and V_c) correspond well with the dependence of direct measurements of the refractive index and thickness of collagen films on the level of their hydration.[40]

3 THEORETICAL BACKGROUND

In this section models for transport of light and matter through a fibrous tissue (samples of human sclera) are presented. The optical models developed show different features of how the effect of matching refractive indices is manifested, and include models for noncoherent and coherent light transportation. The single-scattering model based on Mie theory and including spatial correlation of the scatterers (closely packed, long, dielectric cylinders) is accurate for describing scleral optical properties only for high levels of refractive index matching. Two Monte Carlo simulation techniques are presented that can be used to describe scleral transmission spectra and the distribution of transmitted or backscattered Gaussian light beams. These techniques are valid for a multiple scattering mode and therefore can be used to calculate the optical properties of tissue for all stages of refractive index matching, but they do not take into account the spatial correlation of the scatterers.

The transition from multiple to low-step or single scattering mode due to refractive index matching directed our interest to coherent effects, when a coherent laser beam propagates through a tissue. Using only the most general assumptions about the formation of multiple scattering fields, the random walk theory allows us to qualitatively describe the correlation properties of the far-field speckle structures.

We present three approaches to describing the transport of matter induced by osmotically active chemical agents which leads to matching refractive indices. Each approach has its own area of application. Free diffusion is a quite reasonable approach for describing the transport of many types of molecules through a fibrous tissue. Hindered diffusion through membranes can be used to describe the penetration of molecules into cells and collagen fibrils. The thermodynamic approach is the most suitable for describing osmotic phenomena.
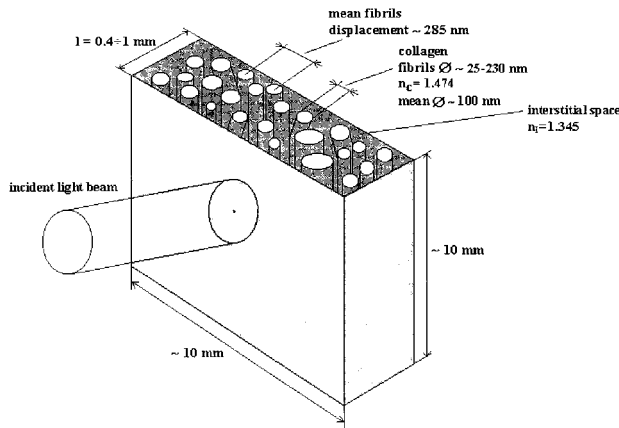
Fig. 1 Schematic representation of the structure of human scleral samples and the geometry of light irradiation.

3.1 LIGHT SCATTERING MODELS AND MEASURING TECHNIQUES

In this subsection light scattering models for transport of noncoherent and coherent light through a scattering medium as well as a calculation and measuring technique for analyzing the interaction of light with fibrous tissue are discussed.

3.1.1 Noncoherent Collimated Light Transmission

The transmission of collimated light by a tissue layer of thickness l is defined as

$$T_c = I/I_0 = \exp(-\mu_t l), \qquad (3)$$

where I_0 and I are the intensities of the collimated incident and detected light, respectively; and $\mu_t = \mu_a + \mu_s$ is the extinction coefficient where μ_a and μ_s are the absorption and scattering coefficients, respectively.

For normal scleral tissue, $\mu_a \ll \mu_s$. For example, for porcine sclera at 633 nm, $\mu_a = 0.2$ mm^{-1}, $\mu_s = 80$ mm^{-1} (see Ref. 32). Moreover, the chemical agents used do not have strong absorbing bands within the wavelength range investigated: 400 to 840 nm. That is why changes in scleral transmittance due to the administration of chemicals can be described only by the behavior of μ_s.

3.1.2 Light Scattering by a System of a Closely Packed, Long, Dielectric Cylinders

Let us consider the optical model of the sclera as a plane plate with a thickness l, which is equal to the local thickness of the sclera. The collagen fibrils will be represented as thin dielectric cylinders with a variety of diameters in the range 25 to 230 nm, and an average diameter of 100 nm, which is considerably smaller than their length. The cylinders' matter has the refractive index $n_c = 1.474$, and the interstitial space is filled by a substance with the refractive index $n_I = 1.345$ (Figure 1). The cylinders are located in planes that are parallel to the plate surfaces, but

within each plane their orientations are random. These simplifications considerably reduce the difficulties in the description of the light scattering of the sclera.

Let us consider the collagen fibril as a thin dielectric cylinder. Light scattering by an individual cylinder can be described by using the Mie theory on the base of the scalar wave equation.[18,19,21,41,42] As a result, the intensity of scattered light for an unpolarized incident plane wave is defined by

$$I_s^1 = |E_s|^2 = (|E_0|^2 / \pi kr)(|T_1|^2 + |T_2|^2), \qquad (4)$$

where E_0 is the amplitude of the incident light, $k = (2\pi n_I / \lambda_0)$ is the wave number; λ_0 is the wavelength of the incident light in a vacuum; r is the distance from the cylinder; T_1 and T_2 are the elements of the amplitude scattering matrix

$$T_1 = b_0 + 2 \sum_{n=1}^{\infty} b_n \cos(n\theta), \qquad (5)$$

$$T_2 = a_0 + 2 \sum_{n=1}^{\infty} a_n \cos(n\theta); \qquad (6)$$

θ is the scattering angle; and a_0, a_n, and b_0, b_n are the coefficients of the expansion into a Mie series.[42] As was shown in Ref. 42, the cross section for light scattering by an individual cylinder can be represented as

$$\sigma_s^1 = \int_0^{2\pi} I_s^1(\theta) r \, d\theta, \qquad (7)$$

which after integrating Eq. (4) allows us to find:

$$\sigma_s^1 = (2/k) \left[|a_0|^2 + |b_0|^2 + 2 \sum_{n=1}^{\infty} (|a_n|^2 + |b_n|^2) \right]. \qquad (8)$$

This solution was obtained for infinitely long cylinders. Nevertheless, it can be successfully used to calculate the scattered intensity in the sclera, because the length of scleral fibrils is much more than their diameters ($\sim 10^5$) and the wavelength ($\sim 10^4$). Equation (8) can be used for computer modeling of the scattered light distribution in the space around an individual fibril. In an approximation of thin cylinders ($x = ka \ll 1$, where a is the cylinder's radius), the scattering cross section for unpolarized incident light is given by[18,19,21]:

$$\sigma_s^1 \cong (\pi a^4 k^3 / 8)(m^2 - 1)^2 [1 + 2/(m^2 + 1)^2], \qquad (9)$$

where $m = n_c / n_I$ is the ratio of the refractive indices of the cylinders and ground materials.

Consequently, for a system of noninteracting thin cylinders with a number of fibrils per unit area ρ_s, the scattering coefficient can be estimated as

$$\mu_s = \rho_s \sigma_s^1 \cong \rho_s (\pi^5 a^4 n_I^3 / \lambda_0^3)(m^2 - 1)^2$$

$$\times [1 + 2/(m^2 + 1)^2], \quad (10)$$

$$\rho_s = w_s / \pi a^2, \quad (11)$$

where w_s is the surface fraction of the cylinders' faces. This expression exactly coincides with that in Ref. 39. As a first approximation it is reasonable to assume that the radii of the scatterers (fibrils) and their density cannot be changed by chemicals and that all variations of μ_s are caused by variations in the refractive index of the interstitial medium, n_I. This allows us to write the ratio of two values of μ_s which correspond to the definite wavelength and to different values of n_I. Because in our case $m \approx 1$, we can find the ratio of the scattering coefficients for different degrees of matching in the approximate form

$$\mu_{s2} \cong \mu_{s1}[(m_2 - 1)/(m_1 - 1)]^2. \quad (12)$$

For example, for $m_1 = 1.1$ and $m_2 = 1.01$, $\mu_{s2} \approx 0.01 \mu_{s1}$; for a close match that is easily attainable in experiments, $m_2 = 1.001$, $\mu_{s2} \sim 10^{-4} \mu_{s1}$. It should be noted that a more rigorous approach to calculating the scattering coefficient must be based on consideration of light scattering by a closely packed system of thin dielectric cylinders.[18,19] Actually, the same approximate expression can be easily derived[10] using the results of Ref. 43 for scattering balls, which is fully discussed in Ref. 8.

A comparison of the results of calculations using the rigorous expressions based on Eq. (8) and the approximations in Eqs. (9) and (10) indicates that for small fibrils with a radius $a = 10$ nm, the discrepancies of the scattering indicatrices $I_s(\theta)$ and σ_s are less than 1% for wavelengths of 400 to 800 nm. Moreover, within small angles (< 10 deg) the indicatrices are very close to each other up to radius $a = 50$ nm. Unfortunately, for σ_s the errors grow very rapidly with the radii of scatterers. For example, for $a = 50$ nm they are, respectively, 61, 18.5, and 10% for wavelengths of incident light of 400, 633, and 800 nm. The error does not exceed 5% for $a = 40$ nm and $\lambda = 800$ nm. The collimated transmission spectra of the scleral layer can be calculated using Eq. (3) for $\mu_a \ll \mu_s$, Eq. (11) for ρ_s, and Eq. (10) or a more rigorous analogous expression based on Eq. (8). In spite of the expected tendency for better transmission at greater wavelengths, the calculated transmission is much lower than the experimental one. For example, calculations for $\lambda = 800$ nm, $a = 50$ nm, and $l = 0.56$ mm give $T_c = 0.01\%$, while the experimental value is about 5 to 13% (see Ref. 6 and Figure 2). Taking into account the portion of light scattered in the forward direction allows us to estimate the total transmission measured in the solid angle Ω
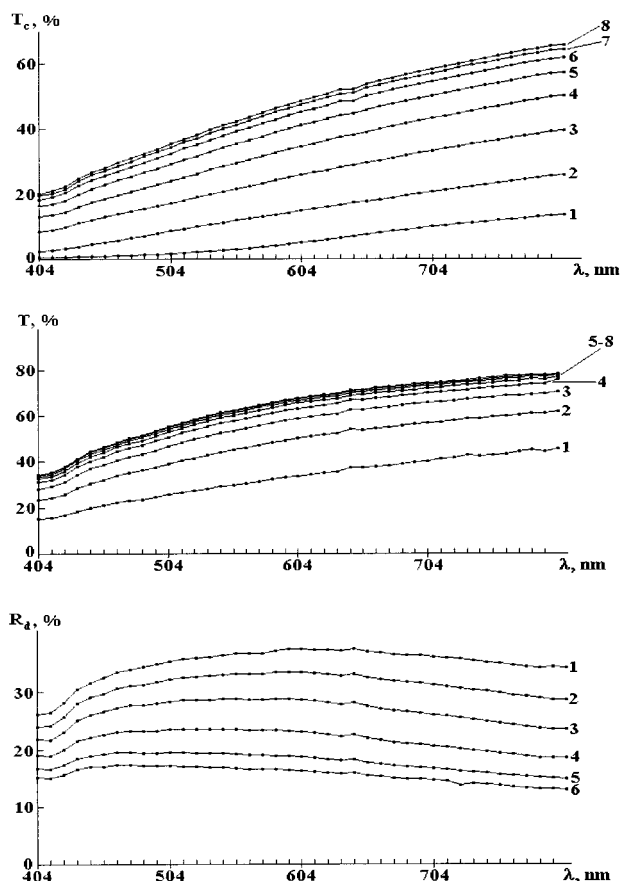

Fig. 2 Typical experimental spectra of the human scleral samples measured for different periods of administration of 60% Trazograph solution. Spectra numbered 1 were measured 1 min after the sample was immersed in solution; spectra 2–8 were measured at 2-min intervals. The measurement time for an individual spectrum, scanning from higher to lower wavelengths, was about 85 s. (a) Collimated transmittance T_c; sample thickness, 0.6 mm. (b) Total transmittance T; sample thickness, 0.7 mm. (c) Diffusion reflection R_d; sample thickness, 0.7 mm (heavy pigmented tissue).

$$T_\Omega = T_c + T_s = \exp(-\mu_s l) + \frac{l}{I_0} \int_0^\Omega I_s(\theta)\, d\theta, \quad (13)$$

where I_0 and $I_s(\theta)$ are, respectively, the intensity of incident and scattered light. Our spectrophotometric measurements for $\theta \approx 30$ deg gave $T_{30} \approx 9\%$ for 800 nm and $l = 0.55$ mm (Figure 3); in comparison, our calculations give only 0.02%. This means that the single-scattering model of a monodispersive system of particles describing the expected tendencies for spectral formation and tissue clearing does not describe these phenomena quantitatively. We need to analyze the model by taking into account various concentration effects that arise in densely packed biological structures, such as interferential interaction between scatterers and multiple scattering in the volume. Because a consistent approach for accounting for the spatial correlation of scattering particles in objects showing multiple scattering has not yet been developed, we consider these two effects separately. Nevertheless, it should be noted
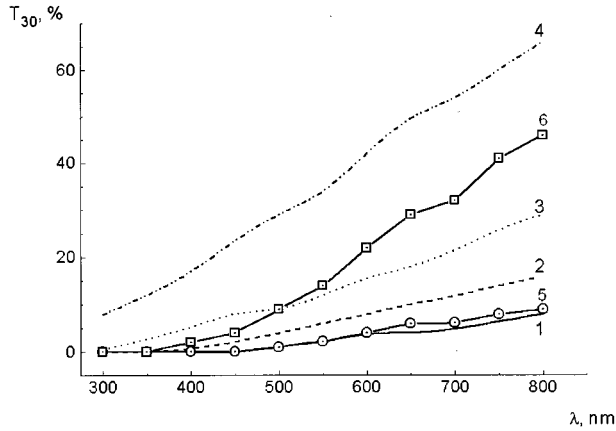
Fig. 3 Calculated (1 to 4) (Monte Carlo simulation) and experimental (5,6) transmission spectra of the human sclera $T_{30}(\lambda)$: 1, $n_l=1.345$; 2, -1.380, 3, 1.410; 4, 1.440; $n_c=1.474$; 5, the untreated scleral sample, $l=0.55$ mm; 6, the same sample after 50 min of Trazograph (60%).

that estimates of the concurrent influence of both phenomena can be made using the approach developed by Kaplan et al.[44]

Owing to the high density of the scleral fibrils, their arrangement must show an order at close distances that causes an interferential interaction of the scattered light. Let us introduce the probability function characterizing the spatial arrangement of the fibrils' centers (the radial distribution function) $g(r)$ as the ratio of the local density of the scattering centers to their mean density.[18,19,21] This function is a key notion in a so-called quasi-crystalline approximation for describing liquids and gels. For the group of N cylinders, the scattered intensity in the far field can be written in the form[18,19,21,39]:

$$I_s = NI_s^1 \left\{ 1 + 2\pi\rho \int_0^R r\,dr [g(r)-1] J_0\left(2k\,\sin\frac{\theta}{2} r \right) \right\}. \tag{14}$$

This equation was first used by the authors of Refs. 18, 19, and 39 to describe corneal transparency. Unfortunately, there are no experimental data for the radial distribution function $g(r)$ for human scleral tissue in the known literature. Possibly it can be found by using the electron micrographs presented in Refs. 33 and 36 through 38 and the calculation method designed by Cox et al.[39] As a first approximation for $g(r)$ we consider an approximation of the excluded volume. That means that there is only one limitation: that particles cannot penetrate each other, but that they are randomly distributed. In that case $g(r)$ has the form:

$$g(r) = \begin{cases} 0, & r<2a \\ 1, & r\geq 2a \end{cases}. \tag{15}$$

Substitution of this into Eq. (14) gives

$$I_s = NI_s^1 \left[1 - 2\pi\rho \int_0^{2a} r J_0\left(2k\,\sin\frac{\theta}{2} r \right) dr \right]. \tag{16}$$

In its turn integration gives

$$I_s = NI_s^1 \left[1 - \frac{2\pi\rho a}{k\,\sin\dfrac{\theta}{2}} J_1\left(4ak\,\sin\frac{\theta}{2} \right) \right]. \tag{17}$$

The approximation of the thin cylinders can be represented as

$$I_s = NI_s^1 \left(1 - 4\pi\rho a^2 + 8\pi\rho a^4 k\,\sin^2\frac{\theta}{2} \right). \tag{18}$$

For the scattering cross section of the systems of N particles,

$$\sigma_s^N = \sigma_s^1 N(1 - 4\pi\rho a^2 + 4\pi\rho a^4 k^2). \tag{19}$$

Using (11) we can rewrite it for an individual cylinder

$$\sigma_s = \sigma_s^1 [1 - 4w_s(1 - a^2 k^2)]. \tag{20}$$

It is important to note that accounting for interferential interaction does not seriously influence the refractive index matching effect, which is defined by σ_s^1 [see Eq. (9)]. Equation (20) can be used to calculate $\mu_s = \rho_s \sigma_s$ and the transmission spectra of tissue $T_c(\lambda)$ and $T_\Omega(\lambda)$ [see Eqs. (3) and (13)]. It is easily seen from Eq. (20) that as a result of the interferential interaction of the scattered light, the cross section σ_s increases for short wavelengths and decreases for long ones. For example, for $a=50$ nm, $w_s=0.3$: $\sigma_s=1.14\sigma_s^1$ (400 nm), $0.4\sigma_s^1$ (600 nm), and $0.14\sigma_s^1$ (800 nm). The calculation of T_c for 800 nm and $l=0.56$ gives $T_c \cong 30\%$, which is about two times more than the corresponding experimental result (see Figure 2). So the interferential effect leads the correction of the transmission spectrum of the sclera in the proper direction, but overestimates the experimental datum. This happened because we did not account for the polydispersity of scatterers (i.e., the sclera was represented as a more ordered tissue, like the cornea) and considered only the model of single scattering. In calculations the approximation of the excluded volume is valid for $w_s<0.1$, and for sclera an estimated value of $w_s \approx 0.3$.

The simplest way to account for multiple scattering is to use the approach suggested by Fine et al.[31] Assuming that for the sclera $\mu_s \gg \mu_a$ (which is a close approximation for untreated sclera),[31,32,45] T_Ω from (13) can be estimated as

$$T_\Omega \cong \exp(-\mu_s l) + (\Omega/2\pi\mu_s l)[1 - (1+\mu_s l)$$
$$\times \exp(-\mu_s l)], \tag{21}$$

where the first term describes as usual the coherent (collimated) light transmission and the second term

describes the incoherent (diffuse) component of transmitted light detected within the solid angle Ω in the forward direction.

For comparison of Eq. (21) with experimental data, we need the corresponding values of μ_s. Experimentally estimated values of μ_s for human sclera are equal to $\cong 41$ mm^{-1} ($\lambda = 633$ nm),[31] and $\cong 25$ mm^{-1} ($\lambda = 670$ nm, measurements using the frequency-domain technique).[45] For a solid angle $\Omega \cong 1$ ($\theta = 30$ deg), $\mu_s = 25$ mm^{-1}, and $l = 0.55$ T_{30} (670 nm)$\cong 1.2\%$. On the other hand, in accounting for the scatterers' spatial correlation, this value underestimates the experimental datum (Figure 3, $T_{30} \cong 5\%$ for $\lambda = 670$ nm). A comparison of these two approaches clearly shows that the only way to quantitatively describe the spectra of the untreated human sclera is to account for both the spatial correlation of scatterers and multiple scattering. Low-step scattering for light propagating in a closely packed tissue such as the cornea or sclera can be included using the approach presented in Refs. 30 and 46. The Monte Carlo simulation technique also is a good way to solve this problem.

3.1.3 Monte Carlo Simulation

Modeling of spectral characteristics of the sclera. Using the probability function for the free photon path l_{ph} (Ref 47):

$$p(l_{ph}) = \mu_t \exp(-\mu_t l_{ph}), \qquad (22)$$

$$\int_0^{l_{ph}} p(l_{ph}) \mathrm{d}l_{ph} = \gamma, \quad 0 < \gamma < 1, \qquad (23)$$

and the Mie phase function calculated for an individual dielectric cylinder, a Monte Carlo simulation was designed for modeling scleral transmission spectra.

Because the random number γ is uniformly distributed in the interval [0,1] the substitution of Eq. (22) into (23) and integrating gives

$$l_{ph} = -\frac{1}{\mu_t} \ln \gamma. \qquad (24)$$

This equation was the basis for modeling photon trajectories, $\mu_t \cong \mu_s$; μ_s is defined by Eqs. (10) or (20), or by more rigorous expressions following from Eqs. (8) and (14). The Mie phase function for noninteracting particles is defined by Eq. (4) and for spatially correlated particles by (14), I_s/N.

This program allows us to calculate collimated, diffuse, and combined transmission spectra of tissues like the sclera and to study refractive index matching effects of interstitial fluid and collagen fibrils.

Modeling of transport of laser beams within tissue. The goal of designing this Monte Carlo simulation program was to find the spatial distribution of light during tissue clearing due to a decrease in the scat-

tering coefficient (caused by refractive index matching). The sclera was modeled as a thin (about 1 mm) homogeneous layer with smooth surfaces. The geometries of the incident beam and detection system corresponded to the experimental arrangement. Two cases were examined: transport of a collimated beam with a radius r and a focused beam with a variable beam waist position regarding tissue depth. Transmitted light was detected on the screen 10 cm from the sample.

The use of a variable stepsize Monte Carlo method with weighing is described in detail by Keijzer.[48] For a collimated incident beam, the source was situated just under the air–tissue boundary; the reflection on the boundary was obtained by setting the photon's initial weight to $(1-R)$, where R is the reflection coefficient determined by Fresnel formulas. For the focused beam, owing to the screen being 10 cm away from the sample, it was possible to ignore the finite dimensions of the beam waist and to use the formulas of geometric optics.

The Henyey–Greenstein function was taken as a single scattering phase function. Parameters μ_a, μ_s, and g, which are needed for modeling untreated sclera, were taken from Hammer et al.[32] and for cleared sclera, values of μ_s were estimated on the basis of our experiments.

The Monte Carlo technique developed includes the possibility of calculating the frequency-domain characteristics of the scattered light, based on the method of weighing described by Yaroslavsky et al.[49]

3.1.4 Coherent Light Propagation through the Sclera

Because scleral tissue shows a large variability in scattering properties due to the refractive index matching effect [see Eqs. (10) and (12)], we should take into account the coherent effects which one expects to dominate in the transparent stage of the tissue. Such consideration is important because it allows us to understand the structural alterations of the tissue caused by chemicals. Space-domain correlation analysis of the scattered light with a transfer of the intensity correlation measurements in the time-domain region seems to have a certain interest for monitoring tissue structure.[50–52] This space-time transfer can be made by scanning the sample with a probe beam and using single-point observation schemes.[51,52]

Using only the most general assumptions about the formation of multiple scattered fields, an analysis of far-zone intensity fluctuations $I_s(t)$ induced by the movement of the steady-structure opaque scattering medium gives the following expression for the intensity autocorrelation function[10,52]

$$g_2(\tau)=\langle I_s(t)I_s(t+\tau)\rangle/\langle I_s^2(t)\rangle$$

$$=\frac{N^2+(N-p)(N-p-1)}{2N^2-N},\qquad(25)$$

where N is the total number of the scattered field contributions induced by sample scanning and detection of the observation point; $p=p(\tau)$ denotes the uncorrelated part of the phasors, which appear to be caused by the displacement of the scattering object in the transverse direction; and τ is the time delay. Equation (25) was performed assuming that the phase shifts arising among different contributions of the scattered field are statistically independent, uniformly distributed random values.

Because in correlation experiments only the fluctuating component $\tilde{I}_s(t)=I_s(t)-\langle I_s(t)\rangle$ of the scattered light intensity is usually determined, the corresponding autocorrelation function can be obtained as:

$$\tilde{g}_2(\tau)=\langle\tilde{I}_s(t)\tilde{I}_s(t+\tau)\rangle/\langle\tilde{I}_s^2(t)\rangle$$

$$=\frac{[N-p(\tau))(N-p(\tau)-1]}{N(N-1)}.\qquad(26)$$

The value of $p(\tau)$, corresponding to the condition $\tilde{g}_2(\tau)=0.5$ and determining the half-width of the normalized autocorrelation peak, is equal to:

$$p_{0.5}=\tfrac{1}{2}[2N-1-(2N^2-2N+1)^{1/2}].\qquad(27)$$

The extreme case of $N=1$ (the average number of the sequences of scattering events, or number of the contributions producing the intensity fluctuations in the observation point is equal to 1), corresponds to the zero value of $p(\tau)$; this case can be examined as the generation of the delta-correlated intensity fluctuations. As $Np(\tau)$ monotonically increases, the asymptotic value of the ratio of $p(\tau)$ to N becomes equal to 0.293.

Taking into account that $\langle I_s\rangle\sim N$ and using Eq. (27), we can find the simple relation between the average intensity of the scattered light for the given direction and the half-width of the autocorrelation function of the far-zone speckle intensity fluctuations, expressed in dimensional form as

$$\Delta\tau_{0.5}=k_1\{2k_2\langle I_s\rangle-1-[2(k_2\langle I_s\rangle)^2-2k_2\langle I_s\rangle+1]^{1/2}\},\qquad(28)$$

where k_1 and k_2 are the model-fitting parameters.

In the region of the small temporal scales, the analysis of the intensity fluctuations can be more precisely carried out by a study of the asymptotic behavior of the corresponding structure function $D_I(\tau)$[53]

$$D_I(\tau)=\langle[I(t+\tau)-I(t)]^2\rangle.\qquad(29)$$

The so-called exponential factor can be used as the generalized parameter for characterizing the behavior of the structure function

$$\nu_1=\frac{\ln[D_I(\tau_2)/D_I(\tau_1)]}{\ln(\tau_2/\tau_1)},\qquad(30)$$

where values of τ_1 and τ_2 determine the boundaries of the region of temporal scales for which ν_1 is estimated.

3.2 FLUID TRANSPORT WITHIN TISSUE

In this subsection, the origin and dynamics of the matching of fibrous tissue refractive indices caused by chemical agents is analyzed. Because of the complex nature of the transport matter within tissue, three different ways of transport are discussed: free, hindered diffusion, and osmotic permeation. The expressions describing the time-dependent concentration of chemical agents within tissue are presented.

3.2.1 Free Diffusion

Owing to the fibrous structure of the sclera, it is quite reasonable to assume that the dynamics of fluid diffusion within this tissue is well described by free diffusion.[54–56] The diffusion equation for the local variation of fluid concentration within a layer can be written in the form[55,56]

$$\frac{\partial c}{\partial t}=D\,\frac{\partial^2 c}{\partial x^2},\qquad(31)$$

where c is the fluid concentration, D is the coefficient of diffusion, and x is the spatial coordinate. This equation is applicable in the cases when the rate of the process is not limited by membranes, such as the diffusion of substances in the interstitial space or when a substance in solution has a high rate of permeation through membranes.[55] The solution of Eq. (31) for a plane plate with a thickness l, which is placed at the moment $t=0$ in a solution with the concentration c_0 (the initial concentration of this substance within the plate is equal to 0, i.e., $t=0$; $0\leqslant x\leqslant l$; $c=0$) has the form[55]

$$c=c_0\Big\{1-\frac{4}{\pi}\,[\exp(-t/\tau)\sin(\pi x/l)+(1/3)$$

$$\times\exp(-9t/\tau)\sin(3\pi x/l)+(1/5)$$

$$\times\exp(-25t/\tau)\sin(5\pi x/l)+...]\Big\},\qquad(32)$$

where

$$\tau=\frac{l^2}{\pi^2 D}.\qquad(33)$$

The ratio of the amount of dissolved matter m_t at the moment t to its equilibrium value m_∞ is defined as[55]

$$m_t / m_\infty = \left(\int_0^l c\, dx \right) \Big/ c_0 l$$

$$= 1 - (8/\pi^2)\{\exp(-t/\tau) + (1/9)$$

$$\times \exp(-9t/\tau) + (1/25)\exp(-25t/\tau)$$

$$+ \dots\}. \tag{34}$$

Equations (32) through (34) allow us to find the time-dependent concentration of chemical agents with a relatively low molecular weight at the depth x of the plane scleral sample or time variations of the relative total amount of these agents within a whole scleral sample if we know the diffusion coefficient D of these molecules in tissue. On the other hand, measurement of $c(t)$ and $m_t(t)$ makes it possible to estimate the D value of implanted molecules in the interstitial fluid of the sclera. For low molecular weight compounds, the values of their diffusion coefficient in their own media are about 10^{-5} cm^{2}s^{-1}; for water, $D = 2.5 \times 10^{-5}$ and 0.5×10^{-5} for saccharose.[55]

3.2.2 Diffusion through Membranes

Based on Fick's first law, which limits the flux of matter $J(\text{mol/s/cm}^2)$ to the gradient of its concentration:

$$J = -D \frac{dc}{dx}, \tag{35}$$

for stationary transport of matter through a thin membrane, we have[55]

$$J = P(c_1 - c_2), \tag{36}$$

where $P = D/l$ is the coefficient of permeability, and c_1 and c_2 are the concentrations of molecules in two spaces separated by a membrane.

Using Eqs. (35) and (36), it is possible to find the variation in concentration of molecules inside a closed space with a volume V surrounded by a permeable membrane with an area S by using the following equation[55]

$$\frac{dc_2}{dt} = \frac{PS}{V}(c_1 - c_2). \tag{37}$$

For a large external volume when c_1 can be considered as a constant, Eq. (37) has an exponential solution

$$c_2 \cong c_1\{1 - \exp(-t/\tau)\}, \tag{38}$$

where

$$\tau = l^2/D. \tag{39}$$

Equation (38) indicates that in our experiments $V = S \times l$, where S and l are the area and thickness of the scleral sample. The form of these equations is very close to that for free diffusion [see Eqs. (32) and (33)], but the values of the diffusion coefficient for free and hindered diffusion can be quite different.

3.2.3 Thermodynamics of Water Transport through a Partly Permeable Membrane

Water may be transported through a membrane (tissue layer) by an increased concentration of dissolved substance in one of two parts of the system. This happens for membranes more permeable for water than for dissolved material and is called osmosis. The simplest case of water transport is when a membrane is permeable for water and totally unpermeable for molecules of dissolved substances. However, in general, biological membranes are permeable for both water and dissolved substances, but the degree of permeability for them can be quite different. This is the most complicated case to describe, but the situation becomes simpler when water and a dissolved substance permeate by the same paths inside a membrane (such as pores in the interstitial space of the sclera, which are filled by the interstitial matter containing water). In that case, fluxes of water and dissolved substance interact and each flux is dependent on the degree of interaction. Such interaction between the stationary fluxes can be well described within the framework of irreversible thermodynamics.

Assuming that in a system there is only one type of dissolved molecule (i.e., two fluxes move through a membrane: the water flux J_W and a dissolved matter J_S, which are proportional to the gradients of the chemical potential of water and dissolved matter), we can find the volumetric flux defined as[55]

$$J_v = J_w \bar{V}_w + J_s \bar{V}_s, \tag{40}$$

where $\bar{V}_W$ and $\bar{V}_S$ are the partial mole volumes, in a form

$$J_v = L_p(\Delta p - \sigma R T \Delta c_s). \tag{41}$$

The flux of dissolved matter can be expressed as[55]

$$J_s = RT\omega\Delta c_s + \tilde{c}_s(1-\sigma)J_v. \tag{42}$$

Here, in Eqs. (41) and (42), L_p is the phenomenological coefficient indicating that the volumetric flux can be induced by rising hydrostatic pressure Δp; σ is the reflection coefficient [$\sigma = -(L_{pd}/L_p)$, where L_{pd} is the phenomenological coefficient indicating on the one hand the volumetric flux that can be induced for the membrane by the osmotic pressure $RT\Delta c_S$, and on the other, the efficiency of the separation of water molecules and dissolved matter]; $\omega = (L_D - L_p\sigma^2)\tilde{c}_S$, where L_D is the phenomenological coefficient characterizing the interchange flux induced by the osmotic pressure $RT\Delta c_S$; and $\tilde{c}_S$ is the average concentration of dissolved matter in two interacting solutions.

For the ideal partly permeable membrane, $\sigma = 1$. For membranes that are permeable for molecules of dissolved matter, $0 < \sigma < 1$. Equations (41) and (42) are valid for solutions with a low concentration. It should be noted that the volumetric flux for a partly permeable membrane described by Eq. (41) has the same mechanism of creation for both hydrostatic and osmotic pressure. So for porous (fibrous) materials (such as the sclera), it is expected that osmotic pressure induces the flux of water due to increasing hydrostatic pressure, but not through independent diffusion of water molecules caused by their concentration gradient, because this entails considerably more resistance.[55]

4 METHODS AND MATERIALS

4.1 SCLERAL SAMPLES

In our study all experiments were performed *in vitro* with human scleral samples. Spectrophotometric measurements were done for 40 samples and correlation intensity experiments were done for samples obtained from 8 autopsy eyes. The ages of the dead ranged from 61 to 72 years. The eyes were prepared immediately after enucleation. The conjunctiva and the ciliary body, as well as the retina with choroid, were removed. The scleral samples were carefully cleaned and cut into pieces of about 10×10 mm². The thickness of the sample was measured with a micrometer and varied from 0.4 to 0.8 mm. Some samples were weighed before and after administration of the chemical agents. Samples were placed in a 1-ml cuvette filled with the chemical agent.

4.2 CHEMICAL AGENTS FOR OPTICAL CLEARING OF THE SCLERA

Three types of chemical agents were chosen for scleral optical clearing. The main part of the experiments were performed using Trazograph (a derivative of 2, 4, 6-triiodobenzene acid) and a water solution of 60 and 76% concentration and a molecular weight of about 500. Some measurements were performed for two osmolytes with quite different molecular weights, such as glucose ($\sim$180) and polyethylene glycol (PEG) (6000 or 20,000).

4.3 REFRACTIVE INDEX MEASUREMENTS AND CALCULATIONS

For the present study it was important to know the refractive indices of different components. We used an Abbe refractometer to measure the refractive indices of the chemical agents. For the Trazograph solutions at room temperature, the measurements were $n = 1.437$ for 60% and 1.460 for 76%, and for the PEG (6000) solutions: $n = 1.368$ (0.4 g/ml), 1.394 (0.6 g/ml), 1.403 (0.8 g/ml), and 1.469 (1.0 g/ml).

For the glucose–water solutions, the refractive index was estimated using the following expressions[6,12,13]:

$$n_g = n_{H_2O} + 0.1515 c_g (\text{g/ml}), \tag{43}$$

$$n_{H_2O} = 1.31848 + 6.662/[\lambda(\text{nm}) - 129.2]. \tag{44}$$

4.4 OSMOTIC PRESSURE MEASUREMENTS

The osmotic pressure of untreated and treated scleral samples was measured using a cryoscopic technique by applying a semiconductor miniature thermoresistor (Karmanov's sensor). The scleral sample with a temperature sensor and the sensitive head inserted into the scleral tissue was put into a refrigerator. The sensor was calibrated using KCl solutions.

4.5 SPECTROPHOTOMETRIC MEASUREMENTS

The spectrophotometric measurements in the wavelength range 400 to 840 nm were obtained with commercially available spectrophotometers, Specord M-40 and Cary-2415. The Specord M-40 spectrophotometer was slightly changed (the sample holder was placed in front of the photomultiplier tube, PMT) in order to obtain mixed transmission spectra measurements for collimated and diffuse light in a solid angle of about 30 deg around the collimated beam. The time period for registration of one spectra was about 5 min. The Cary-2415 spectrophotometer allowed us to measure collimated transmittance, total transmittance, and diffuse reflectance using an integrating sphere. An individual spectrum was registered for 85 s.

For time-dependent measurements at the selected wavelengths, a portable photocolorimeter was used. It was also slightly changed for measurements of collimated light transmission at wavelengths of 450, 500, 600, and 700 nm. A low-power (0.5 mW) He:Ne laser system was also used to measure time-dependent collimated transmission at 633 nm.

4.6 INTENSITY CORRELATION MEASUREMENTS

The optical scheme of the spatial speckle correlometer is described in detail in Refs. 10 and 52. A monomode He:Ne laser (633 nm) was used as a light source; the optical system focused the illuminating beam on a spot with a diameter on the order of 5 μm. The samples under study were usually placed in the waist plane of the illuminating beam and their motion in a direction perpendicular to the beam axis was provided by a 2-D scanning device with step motors. Scanning steps for both directions were equal to 5 μm. Intensity fluctuations of the scattered light produced by the transverse displacements of the studied specimen were detected by the

photomultiplier with a pinhole. An on-axis position of the photodetector corresponding to a zero scattering angle was used in our experiments; the pinhole diameter of 25 μm was much less than the average speckle size for the distance between the PMT and the sample. The wide-band preamplifier and 12-bit A/D converter (DASH-16F, MetraByte Co. U.S.) were used for preliminary signal processing. The maximum scanning speed was about 5 mm/s. A high temporal resolution that allowed us to obtain at least 20 equidistant sampling points for a time interval corresponding to the sample displacement for one scanning step was provided electronically. A CCD camera and video–computer system were used to image the dynamic speckle patterns. This setup also allowed us to study the polarization characteristics of the transmitted light.

5 RESULTS AND DISCUSSION

It will be shown that the human scleral transmission and reflection spectra can be substantially changed by administration of osmotically active chemical agents. For example, if a Trazograph solution (60%) is administered, the collimated transmittance at $\lambda = 800$ nm increases to 75%. Measurements of the time-dependent collimated transmittance allowed us, based on tissue refractive index matching, to estimate the diffusion coefficients of chemical agents used for scleral optical clearing.

The main features of the transition from multiple to low-step scattering of cleared tissue is demonstrated by using spectral and correlation measurements as well as Monte Carlo simulation techniques.

5.1 CONTROL OF HUMAN SCLERAL TRANSMISSION AND REFLECTION SPECTRA USING OSMOLYTES

The human scleral transmission spectra $T_c(\lambda)$ and $T(\lambda)$, and diffusion reflection spectra $R_d(\lambda)$ measured by the spectrophotometer for different time intervals of 60% Trazograph administration, are presented in Figure 2. It is easily seen that the untreated sclera is poorly transparent for visible and NIR light. Trazograph administration makes this tissue highly transparent—up to 75% at 800 nm for the sample kept in solution for $\Delta t = 7$ to 10 min. In addition, its spectral reflectivity decreases from more than 30% to slightly less than 15% in this wavelength range.

In general, for many of measured spectra we can conclude that for untreated scleral samples transmittance was less than 1 to 2% in the range 400 to 500 nm and increased up to 6 to 30% for NIR wavelengths, depending on the sample thickness and pigmentation. Trazograph administration not only leads to increased transmittance but changes the form of the spectral curve: on average, for the short wavelengths transmittance increased from 2 to 20% (10 times) and for the long wavelengths from 20 to 30% to 50 to 80% (about 2.5 times).

For the optically cleared sclera, the collimated light makes the main contribution to transmittance. Direct measurements performed for a scleral sample of 0.75 mm thickness treated with a Trazograph solution for 40 min showed that $T_{30} \cong 35\%$ (400 nm) and $\cong 85\%$ (840 nm), and $T_c \cong 27\%$ (400 nm) and $\cong 85\%$ (840 nm).

For bovine sclera, it was experimentally shown using photocolorimetric measurements that the efficiency of the tissue clearing depends on the concentration and temperature of the solutions used; for room temperature (18.5 °C), the maximum collimated transmittance at 450 nm is in the range $T_{c\max} = 13\%$ (Trazograph, 60%), 22% (glucose, 45%), 39% (Trazograph 76%), 46% (PEG (6000), 80%); and at 700 nm $T_{c\max} = 73\%$ (glucose, 45%), 76% (Trazograph, 60%), 99% (Trazograph, 76%, and PEG, 80%). For example, for a PEG 20,000 solution (80%) the time of maximum tissue clearing changed from 27 min for room temperature to 12 min at physiological temperature ($\sim 38°$C).

The calculated (using the Monte Carlo simulation technique described in Sec. 3.1.3) and experimental spectra presented in Figure 3 show that refractive index matching is the main mechanism responsible for tissue optical clearing. The discrepancy between experimental and theoretical curves (compare Figures 3, 4 and 6) allows us to conclude that the Monte Carlo simulation technique should include the spatial correlation of scatterers, which gives a rapid increase in transmittance with the wavelength.[57]

The Monte Carlo simulation technique developed allows us to describe the transition from complete diffusion to partially coherent transmission of the sclera caused by refractive index matching. Such a transition calculated for collimated transmittance and forward scattering (T_{30}) [see Eq. (13)] for light with $\lambda = 633$ nm is clearly illustrated by the histograms in Figure 4. These histograms show that for untreated sclera (unmatched refractive indices) there is an approximately uniform distribution of the number of scattering events that traveling photons undergo. For fairly matched refractive indices, there are large amounts (about 76%) of ballistic photons (the coherent part of transmitted light), with fractions of 12% single scattered photons, 4% two-step scattered photons, etc.

5.2 TIME RESPONSE OF SCLERAL CLEARANCE: ESTIMATION OF DIFFUSION COEFFICIENT

The time-dependent collimated transmittance of a scleral sample measured at 633 nm concurrently with Trazograph administration is presented in Figure 5. It shows the dynamics of tissue clearing. Similar characteristics were measured for glucose
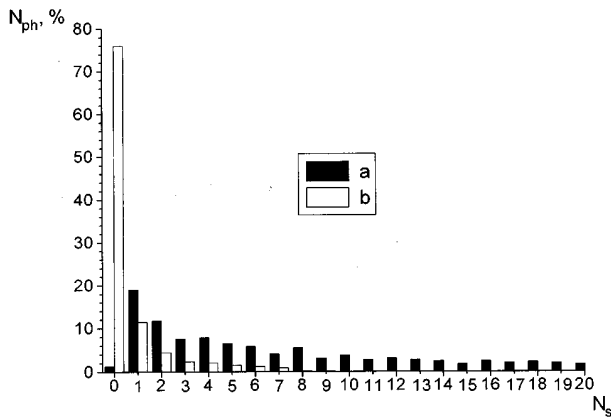
Fig. 4 Histograms of the distribution of the number of scattering events N_s which photons N_{ph} (% of total amount) transmitted (T_{30}) through the sclera undergo. (a) Model of the untreated sclera, n_I = 1.345. (b) Model of partly enlightened sclera, n_I = 1.410, n_C = 1.474, λ = 633 nm.

Table 1 Mean values and rms of diffusion coefficient for Trazograph D_T in the human scleral samples defined on the basis of experimental data for $T_c(t)$, using Eqs. (38) and (45).

Sample	Thickness of sample (mm)	Coefficient of diffusion (cm²/s)	rms of diffusion coefficient (cm²/s)
1	0.5	1.46×10^{-5}	1.90×10^{-6}
2	0.5	4.00×10^{-6}	1.15×10^{-6}
3	0.4	5.29×10^{-6}	7.58×10^{-7}
4	0.4	1.20×10^{-5}	1.01×10^{-6}

and PEG administration. The registration of the dynamic response of the transmission intensity can be used to estimate the diffusion coefficients of the interacting fluids: water and Trazograph, water and glucose, etc. Based on the theoretical background given in Sec. 3, we can estimate the coefficient of diffusion for Trazograph assuming that water and Trazograph have the same paths for diffusion. Using Eqs. (1), (3), and (12), we can find

$$c_T(t) = \frac{1}{n_T - n_I}$$

$$\times \left\{ \frac{n_c}{1 + \left[\frac{n_c}{n_1(0)} - 1 \right] \sqrt{\frac{|\ln T_c(t)| - \mu_a l}{|\ln T_c(0)| - \mu_a l}}} - n_I \right\},$$

$$(45)$$

where n_T is the refractive index of Trazograph, $n_I(0)$ is the refractive index of the interstitial me-
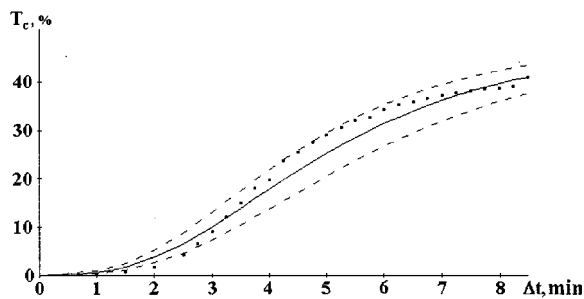

Fig. 5 The time-dependent collimated transmittance (dots) of a 0.5-mm-thick scleral sample measured at 633 nm concurrently with administration of 60% Trazograph. The solid and dashed lines represent the mean value and the upper and lower limits of T_c obtained by a calculation [Eqs. (3), (12), and (38)] of T_c using experimental data: $D_T = 1.46 \times 10^{-5} \pm 1.90 \times 10^{-6}$ cm²/s (see Table 1, sample #1).

dium for $t = 0$, and n_I is the refractive index of the interstitial medium defined by endogenous high molecular weight components and water, $n_I \cong n_I(0)$.

The experimental data like those presented in Figure 5 allow us to use Eqs. (45), (38), (39), and $n_c = 1.474$, $n_w = 1.332$, $n_I(0) = 1.345$, $\mu_a = 0.2$ mm^{-1} to estimate D_T. These data for different samples of the human sclera are collected in Table 1. It is easily seen that estimated values of D_T for some scleral samples have quite reasonable rms errors and differences in D_T mean values are also quite reasonable from sample to sample. It should be noted that mean values and rms errors were calculated using about 30 magnitudes of T_c measured for different time delays for each sample (see Figure 5). As can be seen from Figure 5, rms values include the low-frequency oscillations of $T_c(\Delta t)$, which can be caused by spatial–temporal fluctuations of diffusing matter within tissue. On average, the D_T values are not far from the values of D for diffusion of low-weight molecules in water.[55]

It should be also noted that for the osmolytes studied, fluid transport within tissue is more complicated because there are at least two interacting fluxes, so the model for describing these processes should be more complicated and should include monitoring of additional measurement parameters, such as the refractive index of the chemical agent, tissue weight, and osmotic pressure. Such monitoring of the refractive index of a Trazograph solution (60%) in a process of scleral clearing gave 1.4370 ($\Delta t = 0$), 1.4321 (12 min), 1.4222 (20 min), and 1.4025 (40 min). Unfortunately, the measuring technique used did not allow us to monitor the weight of the sample; we could only measure it before and after administration of the agents. Typical values are the following: Trazograph (60%), sample 1 (5 $\times 8 \times 0.6$ mm³), 54 mg ($\Delta t = 0$), 51 mg (34 min); glucose (40%), sample 2 ($10 \times 11 \times 0.5$ mm³), 82 mg ($\Delta t = 0$), 66 mg (20 min); PEG (6000) (1 g/ml), sample 3 ($8 \times 10 \times 0.5$ mm³), 65 mg ($\Delta t = 0$), 48 mg (60 min).

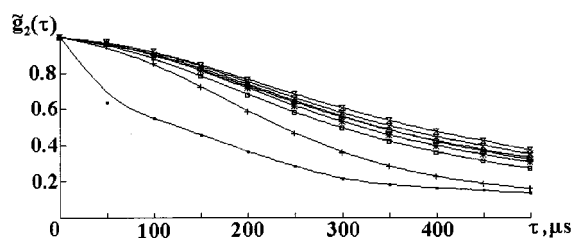Measured values of osmotic pressure for a Trazograph solution were equal to 4.3 MPa (60%) and 7.1

Fig. 6 Evolution of the form of the autocorrelation peak with a decay in scleral turbidity for a 0.55-mm-thick sample. Time periods of signal recording during Trazograph administration: ·, 120 s; +, 220 s; *, 320 s; □, 420 s; ×, 520 s; ◇, 620 s; △, 720 s; ⊠, 820 s.

Fig. 7 Typical dependencies of the exponential factor ν_I (a) and the normalized value of the average intensity $\langle I_s \rangle / I_0$ (b) measured at an observation point during Trazograph administration.

MPa (76%). For untreated sclera, the value of osmotic pressure was equal to 0.74 MPa, and it increased after administration of Trazograph solution for 30 min—up to 5.02 MPa (60%).

5.3 INTENSITY CORRELATION MEASUREMENTS

During the turbidity decay process, the samples under study were scanned by a focused probe beam using a spatial speckle correlometer. The trace length was usually equal to 8 mm. The time interval between two tracing procedures was chosen to provide a recording of the analyzed data with the appropriate time resolution and was usually equal to 1 min. The characteristic changes of the far-zone speckle structure can be seen clearly after Trazograph administration. First there are no visually observed speckles in the far diffraction zone, but after a few minutes (from 1 to 3, depending on the scleral thickness, its initial transmittance, and Trazograph concentration), an isotropic pattern consisting of small-sized speckles appears in the detection plane. For longer periods of time, the speckle pattern becomes inhomogeneous, with the large-sized speckles in the central part. Finally, the main part of the transmitted light is concentrated around the incident beam axis.

Figure 6 shows the evolution of the main correlation peak caused by the transition between two scattering modes for one scleral sample. Specific changes in the nature of the correlation function with an increase in scleral transparency should be noted: for short periods after Trazograph administration (about 1 to 2 min), the normalized autocorrelation function $\langle \tilde{I}(t)\tilde{I}(t+\tau) \rangle / \langle \tilde{I}(t)^2 \rangle$ is rather "exponential"; however, for later stages of transition, another autocorrelation form (closer to Gaussian) is characteristic. In addition, peculiarities such as "multiscality" are observed for scleral specimens with high turbidity (at the initial stages of the process); this is clearly seen in a few characteristic regions of autocorrelation function with significantly differing slopes. The evolution of the form of the main autocorrelation peak caused by variations in
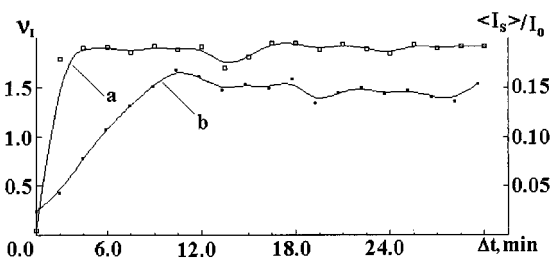
the parameters of scattering particles is illustrated by the typical dependence of ν_I on the time after the administration of the clarifying agent (Figure 7). An exponential factor was estimated for small time scales $\tau = 2 \times 10^{-4}$ s using Eq. (30). The sharp increase in this parameter after the beginning of clearing is obviously associated with the suppression of multiple scattering and can be examined in terms of the decrease in the average number of elementary scattering events for each "chain" of events.[52]

In our case we can interpret movement of a scleral sample as a monovelocity flow of highly concentrated, homogeneously distributed, and randomly oriented anisotropic particles. For tissue in a turbid state (at the early stages of the transition process), with very small inner spatial scales of the scattering structure, scattered light intensity fluctuations are produced by variations in the large amount of statistically independent contributions of the phase factors. For the observation periods used we can see the result as a stochastic process with small values of ν_I. At the final stages, "forward scattering" events are predominant and these conditions are rather close to the single-scattering mode. In this case we can see that the half-widths of the autocorrelation peaks asymptotically increase to values on the order of $(0.3 \text{ to } 0.4) \times 10^{-3}$ s. This characteristic time is closely correlated with the value equal to w/v (w is the waist radius of the illuminating beam and v is the scanning speed). The last parameter can be examined as variations in the time scale of the phase transmittance function if single scattering processes are predominant and the random-phase screen approach can be used to describe the scattered field formation.

Another peculiarity clearly observed, especially at final stages of the process, is the presence of low-amplitude quasi-periodic oscillations of the averaged transmission intensity, the exponential factor ν_I, and the correlation peak half-width with characteristic time scales of about 1.5 to 2.0 min (see Figures 5 through 7). Such quasi-periodic oscillations can be induced by the temporal–spatial inhomogeneity of osmolyte diffusion within the tissue volume. The oscillating character of the tissue response can be explained as a multistep origin of
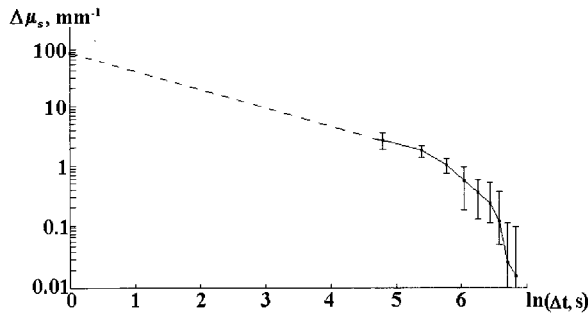
Fig. 8 Evolution of the scattering coefficient variation $\Delta\mu_s$ with decay in scleral turbidity (Δt, period of Trazograph administration).
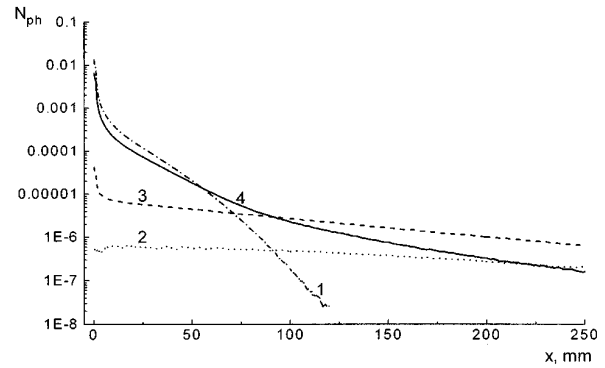

Fig. 9 Calculated average intensity distribution on the plane screen located 30 cm from the scleral sample, beam focused at the front surface of the sample; spot diameter in the waist of Gaussian beam ~ 0.01 mm, $\lambda = 633$ nm, tissue thickness $l = 0.7$ mm, $g = 0.9$, $\mu_a = 0.2$ mm^{-1}. 1, without the sample; 2, $\mu_s = 80$ mm^{-1} (untreated sclera); 3, $\mu_s = 8$ mm^{-1} (partly clarified sclera); 4, $\mu_s = 0.8$ mm^{-1} (partly clarified sclera).

fluid diffusion: at the first step, Trazograph penetration into tissue leads to refractive index matching of interstitial fluid and hydrated fibril collagen, and tissue clearing increases significantly. The second step is characterized by the interaction of Trazograph contained within the renovated interstitial liquid and fibril collagen, which leads to collagen dehydration and a consequent increase in its refractive index that slightly breaks down optical matching and causes a slight decrease in transmittance. An increase in the imbalance of water–Trazograph concentrations leads in turn to penetration of an additional amount of Trazograph into the sample, which causes reestablishment of refractive index matching conditions and corresponding light transmittance; this is the origin of the third step. Such weak oscillations should exist during the total process of chemical administration (up to 40 to 60 min).

Evolution of the sclera's scattering structure due to the "smoothing" of the refractive index fluctuations inside the tissue volume can also be expressed in terms of photon diffusion theory using the values of the scattering and absorption coefficients (μ_s and μ_a). For the geometry of the experiment with fixed conditions, when changes in $\langle I_s \rangle$ are caused only by the variations μ_s, we can write $\langle I_s \rangle / I_0$ as $\langle I_s \rangle / I_0 \sim \exp[(-\mu_t l)] = \exp[(-\{\mu_a + \mu_s\} l)]$ and obtain the dependence of the variation of the scattering coefficient on the period of Trazograph administration (Figure 8). This value was estimated with respect to the asymptotic value of $\langle I_s \rangle / I_0$ and the following expression was used for the estimation procedure: $\Delta\mu_s = -\ln(\{\langle I_s \rangle / I_0\} / \{\langle I_s \rangle / I_0\}_{as}) / l$, where the subscript *as* denotes the asymptotic level of the $\langle I_s \rangle / I_0$ parameter for the later stages of clearing. Averaging was carried out using the experimental results for three different scleral samples obtained from the same autopsy eye. A dashed line is drawn between the first point of this dependence obtained in our experiment (120 s after the beginning of clearing) and the initial value of μ_s characteristic for the human sclera in its initial state (taken from Hammer et al.[32]) (Figure 8). The lower borders of the bar intervals for later stages of the clearing pro-

cess are placed below the (ln Δt) axis; this is the manifestation of the above-mentioned oscillations of $\langle I_s \rangle / I_0$.

5.4 MODELING OF FOCUSED LASER BEAM PROPAGATION THROUGH THE SCLERA WITH CONTROLLED OPTICAL PARAMETERS

The Monte Carlo technique described in Sec. 3.1.3 was used to model propagation of the focused laser beam through a sclera with controlled optical parameters. The geometry of the optical system (laser beam divergence, displacement of the focal plane, thickness of tissue layer, distance between tissue layer and the screen, x) corresponded to that of the experimental setup for the far-zone correlation measurements described in Sec. 4.6. In addition to intensity correlation measurements, this setup allowed us to detect the distribution of average intensity. The dependence of the normalized average intensity on the period of Trazograph administration, as measured in the direction of the incident beam, is shown in Figure 7. The correlation measurements gave the range of variation of μ_s due to Trazograph (Figure 8). These data as well as data from Hammer et al.[32] were used for modeling. The results for 633 nm are shown in Figure 9. It is clearly seen that due to a decrease in μ_s, the coherent peak forms in the central part of the screen. For untreated sclera, the intensity of transmitted light is uniformly distributed on the screen: the incident laser beam is totally destroyed by tissue scattering. The tenfold decrease in the scattering coefficient (partly cleared sclera) leads to the appearance of a small coherent peak in the central part of the screen. The next tenfold decrease in μ_s gives a very pronounced peak, which is even narrower than the initial peak (with-

out sample). This indicates that for transport of focused beams, within a slice of a low-scattering medium ($\mu_s \leqslant 10\ \text{mm}^{-1}$), the scattering process not only forms a wide background illumination of the screen but also induces additional deflection of photons traveling at small angles to the beam axis, which causes narrowing of the central peak of the transmitted light.

6 CONCLUSION

The theoretical and experimental results of this study show that administration of osmolytes to the sclera affects the refractive index matching of the collagen fibrils and interstitial fluid, leading to dramatic changes (a reduction) in the scattering properties of the sclera. For different osmolytes, refractive index matching can be implemented in different ways: (1) water can leave the interstitial space and exit the sample; (2) the administered fluid can enter the tissue and fill up the interstitial space, and water can partly leave the interstitial space and exit the sample. The first mechanism is characteristic for ideal osmolytes, the second, for such osmolytes as PEG, Trazograph, and glucose. Low-amplitude quasi-periodic oscillations of the average transmission intensity and correlation characteristics with the time scale 1.5 to 2.0 min can be induced by the temporal–spatial inhomogeneity of osmolyte diffusion within the tissue volume, which in turn can be caused by the time-dependent reduction of hydration of the fibrils' collagen.

The dynamics of tissue optical clearing using osmolytes is defined by a characteristic time response of about 3 to 10 min. This is in good agreement with results obtained by Rol,[6] but he used mechanical stress or local heating induced by a laser beam. Actually, as follows from Eq. (41), osmotic pressure and hydrodynamic pressure caused, for example, by mechanical stress, have the same mechanism for inducing the fluid flux, and the time response is defined by water diffusion through the interstitial space. So optical clearing using mechanical stress should be equivalent to the action of an ideal osmolyte. From a practical point of view, optical clearing of the human sclera using various osmolytes should be preferable to technology using mechanical stress, because there are more possibilities of controlling the time response using various chemical agents; in addition, the function (tissue clearing and treatment) of these agents can be combined.

Our results are general and can be used to describe many other fibrous tissues. It should be noted that the human sclera can be considered as a living optical etalon that is very sensitive to changes in its structural parameters, but this idea should be supported by a consistent theoretical description that includes molecular and particle (fibril) levels, and accounts for polydispersity and dense packing of scatterers.

The attractiveness of scleral tissue for model experiments with a living tissue lies in the possibility of using chemical agents to affect its scattering properties over a very wide range, which will allow us to understand and describe the transition from a diffuse mode of light scattering to coherent light propagation through tissue. Measurements of light polarization should be very helpful in these investigations.[58–60] The potential of transscleral photocoagulation of the ciliary body in glaucoma therapy using scleral optical clearing by local mechanical compression or laser beam heating are discussed thoroughly by Rol.[6] *In vivo* optical enlightening of rabbit sclera using such osmolytes as Verographin was done by Bakutkin and coauthors.[5] A direct histological study showed that there are no serious irreversible changes in the cellular and fibrous structure of the human sclera for a rather long period of osmolyte administration.[60] For example, for a Trazograph solution (60%), this time is about 30 min. Therefore we expect that a new technology for optical clearing of the human sclera using a suitable osmolyte will be helpful in various clinical applications, including therapy and noninvasive diagnostics.

REFERENCES

1. V. V. Tuchin, Ed., *Tissue Optics: Applications in Medical Diagnostics and Therapy*, SPIE Milestone ser. MS102, Bellingham, WA (1994).
2. E. P. Zege, A. P. Ivanov, and I. L. Katsev, *Image Transfer Through a Scattering Medium*, Springer-Verlag, Berlin (1991).
3. A. P. Ivanov, V. A. Lojko, and V. P. Dik, *Light Transportation in Densely Packed Dispersive Media*, Nauka i Technika, Minsk (1988).
4. V. V. Tuchin, "Laser light scattering in biomedical diagnostics and therapy," *J. Laser Appl.* **5** (2,3), 43–60 (1993).
5. V. V. Bakutkin, I. L. Maksimova, P. I. Saprykin, V. V. Tuchin, and L. P. Shubochkin, "Light scattering of human eye sclera," *J. Appl. Spectroscopy (USSR)* **46** (1), 104–107 (1987).
6. P. O. Rol, "Optics for Transscleral Laser Applications," D. N. Sci diss., Institute of Biomedical Engineering, Zürich, Switzerland (1992).
7. B. Chance, H. Liu, T. Kitai, and Y. Zhang, "Effects of solutes on optical properties of biological materials: models, cells, and tissues," *Anal. Biochem.* **227**, 351–362 (1995).
8. H. Liu, B. Beauvoit, M. Kimura, and B. Chance, "Dependence of tissue optical properties on solute-induced changes in refractive index and osmolarity," *J. Biomed. Opt.* **1**, 200–211 (1996).
9. B. Grzegorzewski and S. Yermolenko, "Speckle in far-field produced by fluctuations associated with phase separation," *Proc. SPIE* **2647**, 343–349 (1995).
10. V. V. Tuchin, I. L. Maksimova, D. A. Zimnyakov, I. L. Kon, A. H. Mavlutov, and A. A. Mishin, "Light propagation in

tissues with controlled optical properties,'' *Proc. SPIE* **2925**, 118–142 (1996).

11. V. V. Tuchin, I. L. Maksimova, V. I. Kochubey, I. L. Kon, A. H. Mavlutov, A. A. Mishin, S. V. Tuchin, and D. A. Zimnyakov, ''Optical and osmotic properties of human sclera,'' *Proc. SPIE* **2979–2996** (1997).

12. J. S. Maier, S. A. Walker, S. Fantini, M. A. Franceschini, and E. Gratton, ''Possible correlation between blood glucose concentration and the reduced scattering coefficient of tissues in the near infrared,'' *Opt. Lett.* **19**, 2062–2064 (1994).

13. M. Kohl, M. Cope, M. Essenpreis, and D. Bocker, ''Influence of glucose concentration on light scattering in tissue-simulating phantoms,'' *Opt. Lett.* **19**, 2170–2172 (1994).

14. C.-L. Tsai and J. M. Fouke, ''Non-invasive detection of water and blood content in soft tissue from the optical reflectance spectrum,'' *Proc. SPIE* **1888**, 479–486 (1993).

15. J. Dillon, ''The photophysics and photobiology of the eye,'' *J. Photochem. Photobiol. B: Biology* **10**, 23–40 (1991).

16. T. W. King, G. L. Cote, R. McNichols, and M. J. Goetz, ''Multispectral polarimetric glucose detection using a single pockels cell.'' *Opt. Eng.* **33**, 2746–2753 (1994).

17. A. V. Priezzhev, V. V. Tuchin, and L. P. Shubochkin, *Laser Diagnostics in Biology and Medicine*, Nauka, Moscow, (1989).

18. D. E. Freund, R. L. McCally, and R. A. Farrell, ''Effects of fibril orientations on light scattering in the cornea,'' *J. Opt. Soc. Am. A.* **3**, 1970–1982 (1986).

19. R. A. Farrell, D. E. Freund, and R. L. McCally, ''Research on corneal structure,'' *Johns Hopkins Appl. Physics Lab. Tech. Dig.* **11** (1,2), 191–199 (1990).

20. H. S. Dhadwal, R. R. Ansari, and M. A. DellaVecchia, ''Coherent fiber optic sensor for early detection of cataractogenesis in a human eye lens,'' *Opt. Eng.* **32**, 233–238 (1993).

21. I. L. Maksimova, V. V. Tuchin, and L. P. Shubochkin, ''Polarization features of eye's cornea,'' *Optics Spectroscopy (USSR)* **60** (4), 801–807 (1986).

22. I. L. Maksimova, V. V. Tuchin, and L. P. Shubochkin, ''Scattering matrix of eye's lens,'' *Optics Spectroscopy (USSR)* **65**, 615–620 (1988).

23. B. K. Piercionek, ''Aging changes in the optic elements of the eye,'' *J. Biomed. Opt.* **1** (2), 147–156 (1996).

24. V. V. Tuchin, ''Fundamentals of low-intensity laser radiation interaction with biotissues: dosimetry and diagnostical aspects,'' *Bull. Russ. Acad. Sci., Physical Ser.* **59** (6), 120–143 (1995).

25. P. Rol, P. Niederer, U. Dürr, P.-D. Henchoz, and F. Fankhauser, ''Experimental investigation on the light scattering properties of the human sclera,'' *Laser Light Ophthalmol.* **3**, 201–212 (1990).

26. F. Veretout, M. Delaye, and A. Tardieu, ''Molecular basis of the eye lens transparency. Osmotic pressure and x-ray analysis of α-crystallin solutions,'' *Mol. Biol.* **205**, 713–728 (1989).

27. D. Maurice, ''The cornea and sclera,'' in *The Eye*, H. Davison, Ed., Marcel Dekker, New York, pp. 489–600 (1969).

28. M. Spitznas, ''The fine structure of human scleral collagen,'' *Am. J. Ophthalmol.* **71** (1), 68–75 (1971).

29. N. I. Zatulina, ''A quantitative analysis of age peculiarities of scleral parameters in man,'' *Ophthalmol. J. (USSR)*, **N5**, 300–303 (1988).

30. V. V. Bakutkin, I. L. Maksimova., T. N. Semyonova, V. V. Tuchin, and I. L. Kon, ''Controlling of optical properties of sclera,'' *Proc. SPIE* **2393**, 137–141 (1994).

31. I. Fine, E. Loewinger, A. Weinreb, and D. Weinberger, ''Optical properties of the sclera,'' *Phys. Med. Biol.* **30**, 565–571 (1985).

32. M. Hammer, A. Rogan, D. Schweitzer, and G. Müller, ''Optical properties of ocular fundus tissues in an in vitro study using double integrating sphere technique and inverse Monte Carlo simulation,'' *Phys. Med. Biol.* **40**, 963–978 (1995).

33. Y. Komai and T. Ushiki, ''The three-dimensional organization of collagen fibrils in the human cornea and sclera,'' *Invest. Ophthal. Vis. Sci.* **32**, 2244–2258 (1991).

34. S. G. Legeza and A. I. Privalov, ''The optimal spatial-temporal characteristics of laser irradiation and experimental application,'' *Ophthalmic J. (USSR)* **N3**, 170–173 (1985).

35. K. Trier, S. B. Olsen, and T. Ammitzbøll, ''Regional glycosaminoglycans composition of the human sclera,'' *Acta. Ophthalmol.* **69**, 304–306 (1990).

36. E. S. Avetissow, L. D. Andreeva, and I. P. Choroshilova-Maslova, ''Electron microscopy study of the human sclera in various aging groups,'' *Ophthalmol. Bull. (USSR)* **N1**, 24–30 (1979).

37. A. Thale and B. Tillman, ''The collagen architecture of sclera. SEM and immunohistochemical studies,'' *Anat. Anz.* **175**, 215–220 (1993).

38. S. Vaezy and J. I. Clark, ''Quantitative analysis of the microstructure of the human cornea and sclera using 2D Fourier methods,'' *J. Microscopy* **175** (**Pt.** 2), 93–99 (1994).

39. J. L. Cox, R. A. Farrell, R. W. Hart, and M. E. Langham, ''The transparency of the mammalian cornea,'' *J. Physiol.* **210**, 601–616 (1970).

40. X. Wang, T. E. Milner, M. C. Chang, and J. S. Nelson, ''Group refractive index measurement of dry and hydrated type I collagen films using optical low-coherence reflectometry,'' *J. Biomed. Opt.* **1** (2), 212–216 (1996).

41. H. C. van der Hulst, *Light Scattering by Small Particles*, Dover, New York (1981).

42. C. F. Bohren and D. R. Huffman, *Absorption and Scattering of Light by Small Particles*, Wiley, New York (1983).

43. R. Graaff, J. G. Aarnoudse, J. R. Jijp, P. M. A. Sloot, F. F. M. de Mul, J. Greve, and M. H. Koelink, ''Reduced light-scattering properties for mixtures of spherical particles: a simple approximation derived from Mie calculations,'' *Appl. Opt.* **31**, 1370–1376 (1992).

44. P. D. Kaplan, A. D. Dinsmore, A. G. Yodh, and D. J. Pine, ''Diffuse-transmission spectroscopy: a structural probe of opaque colloidal mixtures,'' *Phys. Rev. Lett.* **50**, 4827–4835 (1994).

45. L. O. Svaasand, B. J. Tromberg, R. C. Haskell, T.-T. Tsay, and M. W. Berns, ''Tissue characterization and imaging using photon density waves,'' *Opt. Eng.* **32**, 258–266 (1993).

46. T. W. Smith, ''Multiple scattering in the cornea,'' *J. Mod. Opt.* **35**, 93–101 (1988).

47. H. W. Jentink, F. F. M. de Mul, R. G. A. M. Hermsen, R. Graaff, and J. Greve, ''Monte Carlo simulations of laser doppler blood flow measurements in tissue,'' *Appl. Opt.* **29**, 2371–2381 (1990).

48. M. Keijzer, *Light Transport for Medical Laser Treatments*, Technical University of Delf, The Netherlands (1993).

49. I. V. Yaroslavsky, A. N. Yaroslavsky, V. V. Tuchin, and H.-J. Schwarzmaier, Effect of the scattering delay on time-dependent photon migration in turbid media, ''*Appl. Opt.* **36** (1997).

50. V. V. Tuchin, Ed., *Coherence Domain Methods in Biomedical Optics, Proc. SPIE* **2732** (1996).

51. D. A. Zimnyakov, V. V. Tuchin, A. A. Mishin, I. L. Kon, and A. N. Serov, ''In vitro human sclera structure analysis using tissue optical immersion effect,'' *Proc. SPIE* **2673**, 233–242 (1996).

52. D. A. Zimnyakov, V. V. Tuchin, and A. A. Mishin, ''Spatial speckle correlometry in applications to tissue structure monitoring,'' *Appl. Opt.* **36**, 5594–5607 (1997).

53. S. M. Rhytov, Yu. A. Kravtsov, and V. I. Tatarsky, *Introduction to Statistical Radiophysics*, Vol. 2, *Random Fields*, Nauka, Moscow (1978).

54. P. M. A. Sloot, A. G. Hoekstra, and C. G. Figdor, ''Osmotic response of lymphocytes measured by means of forward light scattering: theoretical considerations,'' *Cytometry* **9**, 636–641 (1988).

55. A. Kotyk and K. Janacek, *Membrane Transport: an Interdisciplinary Approach*, Plenum Press, New York (1977).

56. R. David, *Biophysique 1/Biophysique generale*, Presses Universitaires de France, Paris (1979).

57. V. V. Tuchin and D. M. Zhestkov, ''Tissue structure and eye lens transmission and scattering spectra,'' *Proc. SPIE* **3053**, 123–128 (1997).

58. V. V. Tuchin, ''Coherent and polarimetric technologies for the analysis of tissue structure (overview),'' *Proc. SPIE* **2981** 120–159 (1997).

59. D. A. Zimnyakov, V. V. Tuchin, and K. V. Larin, ''Speckle patterns polarization analysis as an approach to turbid tissues structure monitoring,'' *Proc. SPIE* **2981** 172–180 (1997).
60. I. L. Kon, V. V. Bakutkin, N. V. Bogomolova, S. V. Tuchin, D. A. Zimnyakov, and V. V. Tuchin, ''Trazograph influence on osmotic pressure and tissues' structures of human sclera,'' *Proc. SPIE* **2971**, 198–206 (1997).
61. V. V. Tuchin, T. G. Anishchenko, A. A. Mishin, and O. O. Soboleva, ''Control of bovine sclera optical characteristics with various osmolytes,'' *Proc. SPIE* 2982 (1997).